Acta Geodyn. Geomater., Vol. 18, No. 4 (204), 415–428, 2021
DOI: 10.13168/AGG.2021.0029
journal homepage: https://www.irsm.cas.cz/acta

ORIGINAL PAPER

EXPERIMENTAL INVESTIGATION ON PERMEABILITY IN FRACTURED ROCK UNDER DIFFERENT PRESSURE CONDITIONS

Yu ZHANG [1, 2] *, Tingting YU [1], Tong ZHANG [3], Yun JIA [4] and Zongnan ZHANG [1]

[1] *College of Pipeline and Civil Engineering, China University of Petroleum, Qingdao, 266555, China*
[2] *Shandong Key Laboratory of Civil Engineering Disaster Prevention and Mitigation, Shandong University of Science and Technology, Qingdao 266590, China*
[3] *State Key Laboratory of Mining Response and Disaster Prevention and Control in Deep Coal Mines, Anhui University of Science and Technology, Huainan 232001, China*
[4] *Univ. Lille, CNRS, Centrale Lille, UMR 9013 - LaMcube - Laboratoire de Mécanique, Multiphysique, Multi-échelle, F-59000 Lille, France*

**Corresponding author's e-mail:* zhangyu@upc.edu.cn

ARTICLE INFO

Article history:
Received 8 February 2021
Accepted 23 July 2021
Available online 8 October 2021

Keywords:
Different pressure conditions
Fractured rock
Permeability
Permeability model

ABSTRACT

Oil and gas are the main reserves in the fractures of rocks. Under different pressure conditions, fracture permeability of reservoir rock directly affects the flow of oil and gas, which is an important object of oil and gas exploration and development. The permeability of single fractured rock and double fractured rock under different pressure conditions was studied by using high-precision hydro-mechanics coupled triaxial experimental equipment. The experimental scheme is as follows: (i) permeability test under increasing confining pressure, (ii) permeability test under increasing liquid pressure, (iii) permeability test under cyclic loading and unloading deviatoric stress and (iv) permeability test under synchronously increasing confining pressure and deviatoric stress. Results show that the entire change of permeability is irreversibly reduced. This is due to the presence of residual factors in permeability after the dilation cycle and the recompaction cycle ends. On the basis of the dual medium model of fracture, the permeability model of fractured rock is proposed considering the interaction among fracture system, matrix system and expansion deformation of fracture under external stress. The simulation results of the model are in good agreement with the experimental results. These results can provide an important basis for the prediction of permeability of fractured rock and efficient oil and gas exploitation.

1. INTRODUCTION

Knowledge of changes in the hydraulic behaviour of rock fractures that result from the redistribution of stresses around oil and gas projects is crucial. As the main reservoir space and flow channel of oil and gas reservoirs, the permeability change of fractured rocks is an important indicator of reservoir evaluation (Liang et al., 2021; Alexandra et al., 2018; Huo and Benson, 2016; Zhu and Wong, 1997). Hydraulic fracturing and acidification are important methods to enhance their permeability by fracturing deep geological rock formations and improve oil and gas production efficiency (Zhang et al., 2019; Wanniarachchi et al., 2018; Durant et al., 2016; Estrada and Bhamidimarri, 2016). These methods can improve the conductivity of reservoirs by changing the fracture characteristics, thereby accelerating oil and gas flow and increasing oil and gas production (Wang et al., 2018; Liu et al., 2010). Fractured rocks in deep reservoirs under different geological environment of high geo-stress and high liquid pressure significantly affect the mechanical behaviour of deep oil and gas reservoirs, especially for the permeability of reservoir fractured rocks (Katsuki et al., 2019; Zhao et al., 2019). Given that fractures generally have crack-like shapes, they are more susceptible to stress than porous rocks, causing liquid behaviour in fractures to be strongly pressure dependent. The fractures in the rock are easy to close, open and develop under the effect of geo-stress and tectonic stress. Moreover, the fracture permeability is much larger than the pore permeability and is dominant in reservoir rock permeability. Therefore, the permeability of fractures in different pressure conditions remarkably influences production values (Yang et al., 2019; Wan et al., 2013; Abass et al., 2009).

Permeability behaviour is more a "process" than a "material" property (e.g. stress and deformation) (Heiland and Raab, 2001; Heiland, 2003; Liu et al., 2015). Thus, rock permeability depends strongly on the geometry and distribution of fracture within the rock material and on external boundary conditions (e.g. prevailing stress environment) (David et al., 2001; Souley et al., 2001; Gutierrez and Lewis, 2002; Zhang et al., 2007). In addition, the effect of liquid flow reduces the bonding strength of mineral particles and causes fracture to expand and propagate. Thus, the width and quantity of fracture are changed, forming a dynamic flow channel. Laboratory tests have been

Cite this article as: Zhang Y, Yu T, Zhang T, Jia Y, Zhang Z: Experimental investigation on permeability in fractured rock under different pressure conditions. Acta Geodyn. Geomater., 18, No. 4 (204), 415–428, 2021. DOI: 10.13168/AGG.2021.0029

Fig. 1 Single-fractured rock(S1) and double-fractured rock(S2) sample.

conducted to estimate the permeability behaviour of a fractured rock under triaxial loading conditions. The permeability increases with increasing inelastic strain in low-porosity granite (Brace, 1978; Mitchell and Faulkner, 2008) and volcanic rock (Farquharson et al., 2016). The change of permeability with differential pressure can reflect the compression, weakening and failure characteristics of fractured rocks in a compressive state (Wang et al., 2014). However, these reports focus on the permeability change during single loading process. Few studies have investigated permeability change during unloading process and in different pressure conditions; such works investigated the effect of cyclic loading and confining pressure on permeability and heat transfer properties, and the flow and heat transfer characteristics of water flow in rock fractures at high temperature under different pressure conditions are determined (Ma et al., 2019; Shu et al., 2020). The permeability variations of fractured rock in different pressure conditions need to be further studied.

Generally, reservoir rock has a complex internal structure and contains many fractures. Deep reservoirs are prone to stress concentration, which evidently modifies the fracture surface and pore structures of rock. However, accurately describing changes in the permeability of rock fractures is an issue that has not been completely resolved, especially in different pressure conditions. This study aims to quantify the permeability of fractured rock samples in different pressure conditions (e.g. geo-stress, liquid pressure, cyclic loading and unloading deviatoric stress). A permeability model which considers the interaction among fracture system, matrix system and expansion deformation of fracture is proposed.

2. SAMPLE PREPARATION AND EXPERIMENTAL PROCEDURES

2.1. FRACTURED ROCK SAMPLE PREPARATION

The rock sample was cored from outcrop intact rock blocks of an oil and gas project in southwestern China (Fig. 1). The sample was a brittle sedimentary rock with a reddish colour. Cylinder samples, with an average sample size of 25 mm (diameter) × 50 mm (height), were used. The samples were characterized by a good uniformity and cemented contacts and a dense texture without obvious bedding. Physical property tests indicated that the average natural density and porosity were 2.54 g/cm^3 and 3.5 %, respectively. The sample consisted of quartz (87 %), feldspar (5 %), debris (3 %), clay (3 %), and a small amount of iron minerals (2 %). The morphology of fractures plays a key role in governing fractured rocks permeability. The fractured rock samples, namely, single-fractured sandstone sample (S1) and double-fractured rock sample (S2), were created using a water-jet cutting system (Fig. 1). The influence of fracture roughness on permeability is neglected in the present paper and will be discussed in a future study.

2.2. EXPERIMENTAL PROCEDURE

All permeability tests were performed in different pressure conditions by using an auto-compensated and auto-equilibrium triaxial cell system (Fig. 2). The system was composed of a conventional triaxial cell, which can control the confining pressure and the deviatoric stress, and a liquid injection pump which can generate liquid flow pressures on the lower and upper sides of the sample. The maximum confining pressure and axial stress were 60 MPa and 600 MPa, respectively. The maximum liquid flow pressure can reach 30 MPa. Two permeable panels, which were steel plates with evenly distributed holes, were installed respectively on the upper and lower extremities of the sample. Before being placed in the testing cell, the fractured rock samples were sealed using plastic insulation tape and thermal shrinkage plastic top wraps.

Permeability test was conducted in a manner similar to a normal triaxial compression test under drained conditions at room temperature (25±1.5 °C) (Zhang et al., 2015; Zhang et al., 2016). The confining pressure and axial stress were imposed at a constant rate of 0.75 MPa/min and the liquid medium used was

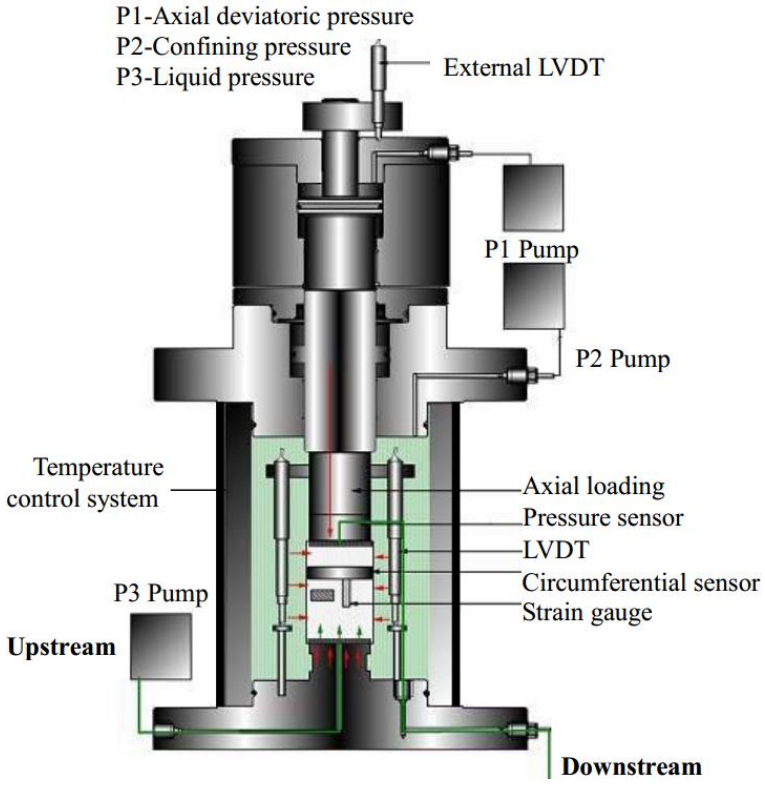

Fig. 2 Self-equilibrium triaxial pressure system of rock servo-controlled triaxial equipment.

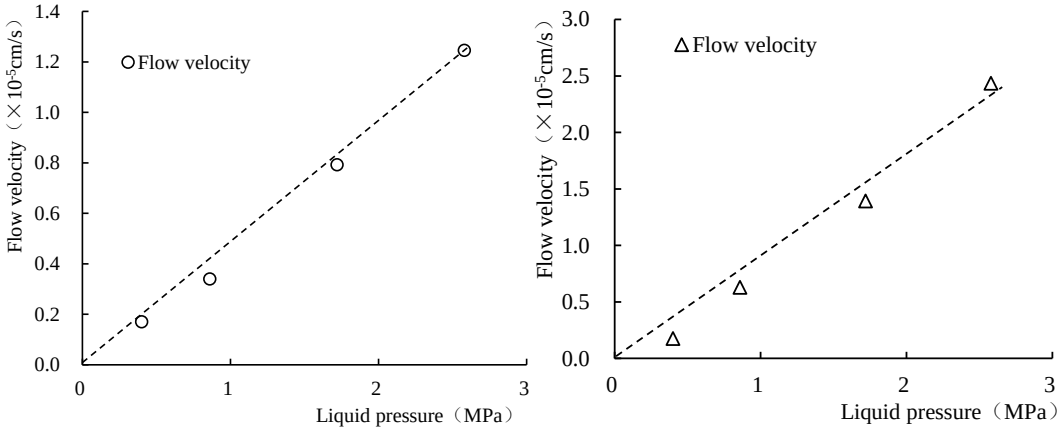

Fig. 3 Relationship between flow velocity and liquid pressure of fractured rock

distilled water. All samples were pre-tested under fully saturated conditions with water in vacuum. The liquid flow pressure gap between the two ends of the sample was supplied by the injection pump. The water flow in the sample could be recorded when the stress state was stable. In general, the rock fracture has strong water-conducting ability, and the liquid flow of fractured rock samples remain in the fracture. The relationship between the flow pressure and flow velocity of S1 and S2 are basically linear when the tests reach stability (Fig. 3). Moreover, the steady state flow method is highly precise and acceptable for permeability values larger than 10^{-19} m^2 (Yang et al., 2010; Heap et al., 2018). Therefore, the steady-state method was employed to measure the permeability of fractured rock samples during triaxial compression.

The permeability test of a single sample in different pressure conditions was performed on single-fractured rock (S1) and double-fractured rock (S2). The test scheme of the pressure condition includes: (i) permeability test under increasing confining pressure, (ii) permeability test under increasing liquid pressure, (iii) permeability test under cyclic loading and unloading deviatoric stress and (iv) permeability test under synchronously increasing confining pressure and deviatoric stress.

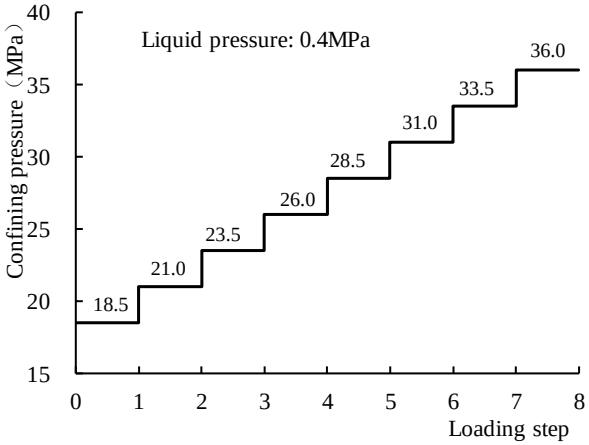

Fig. 4 Scheme of permeability test during increasing confining pressure

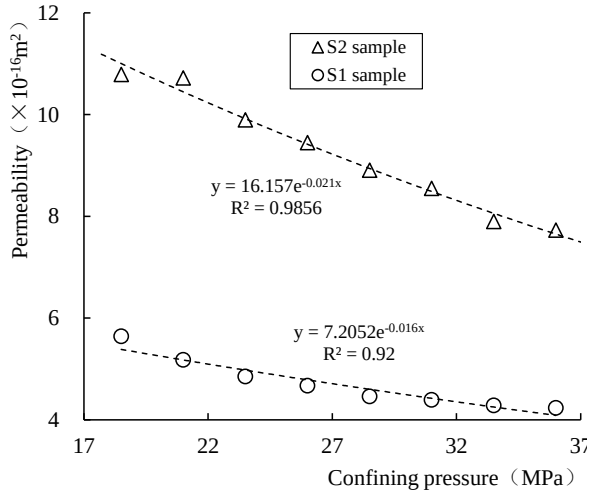

Fig. 5 Permeability evolution during increasing confining pressure.

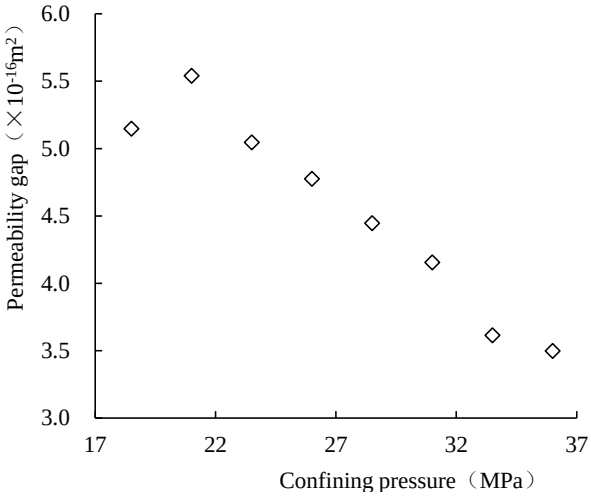

Fig. 6 Permeability gap between S1 and S2 during increasing confining pressure.

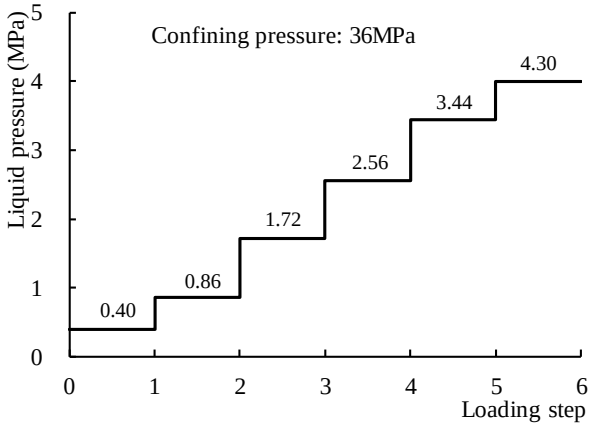

Fig. 7 Scheme of permeability test during increasing liquid pressure.

3. RESULTS OF PERMEABILITY TESTS ON FRACTURED ROCKS IN DIFFERENT PRESSURE CONDITIONS

3.1. PERMEABILITY TEST UNDER INCREASING CONFINING PRESSURE

Permeability measurement during increasing confining pressure was first performed (Fig. 4). The confining pressure increased from 18.5 MPa to 36 MPa with an increment of 2.5 MPa. The liquid pressure of 0.4 MPa was constant during increasing confining pressure. In general, the existing fracture significantly affects the permeability. The results clearly show that the permeability of the double-fractured rock (S2) sample is higher than that of the single-fractured rock (S1) sample (Fig. 5).

The fracture is the main channel of liquid flow. As the confining pressure increases, the width of fractures decreases, which leads to an exponentially decrease in permeability and finally the permeability tends to be stable. At this stage, the initial permeability values of S1 and S2 are 5.64×10^{-16} m^2 and 10.79×10^{-16} m^2, respectively (confining pressure: 18.5 MPa, liquid pressure: 0.4 MPa). When the confining pressure increased to 36 MPa, the permeability values of S1 and S2 decreased by 25 % and 28 %, respectively. The permeability reduction in S2 sample compared with that in S1 sample is significant. The permeability gap between S1 and S2 is gradually decreasing (Fig. 6). This result indicates that the effects of fracture type on permeability change decrease with increasing confining pressure, and the stress sensitivity of permeability of S2 is higher than that of S1.

3.2. PERMEABILITY TEST UNDER INCREASING LIQUID PRESSURE

The second permeability measurement phase is performed with the increase of liquid pressure from 0.4 MPa to 4.3 MPa while constantly maintaining the confining pressure at 36 MPa (Fig. 7). The liquid pressure increase can open and expand the fracture. As

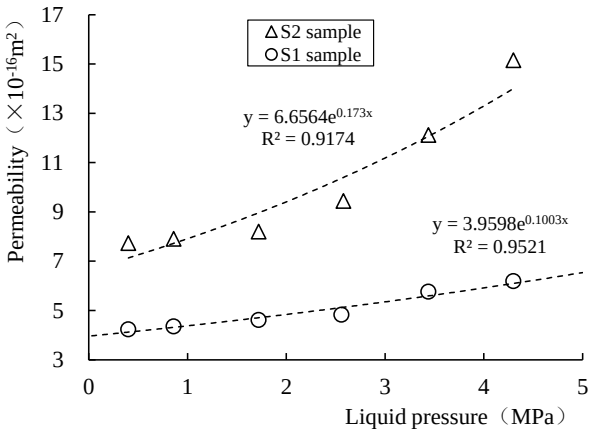

Fig. 8 Permeability evolution during increasing liquid pressure.

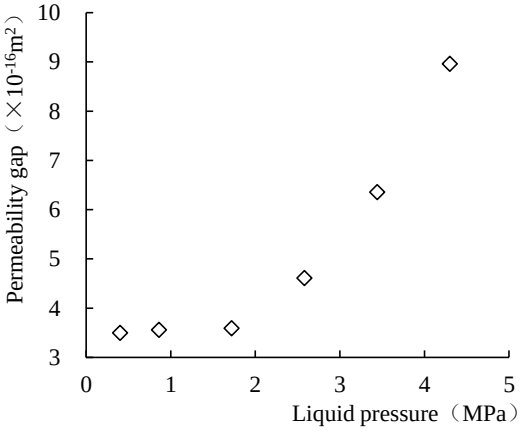

Fig. 9 Permeability gap between S1 and S2 during increasing liquid pressure.

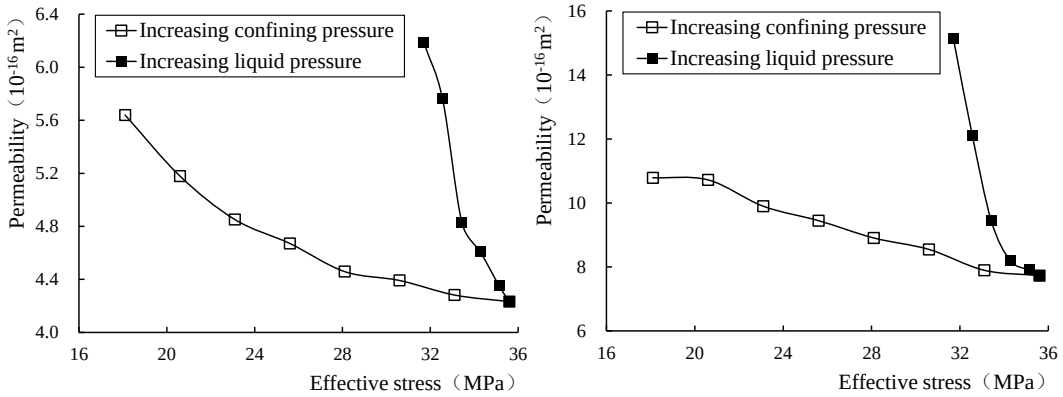

Fig. 10 Permeability evolution during changing effective stress.

the liquid pressure increases, the permeability tends to grow exponentially with the enlarged flow channel (Fig. 8). The initial permeability values of S1 and S2 at this stage are 4.23×10^{-16} m^2 and 7.73×10^{-16} m^2, respectively (confining pressure: 36.0 MPa, liquid pressure: 0.4 MPa). When the liquid pressure increased to 4.3 MPa, the permeability values of S1 and S2 rose by 46 % and 96 %, respectively. The permeability increase rate of S2 is larger than that of S1. The permeability gap between S1 and S2 is rapidly increasing (Fig. 9), indicating that the effect of fracture type on permeability increase is becoming gradually evident with increasing liquid pressure.

Effective stress indicates the difference between confining pressure and liquid pressure. And the liquid pressure in the fracture is equal to the inlet liquid pressure. The permeability of the fractured rock is highly stress dependent, and the effective stress greatly drives permeability variations (Fig. 10). The permeability decreases as the fracture aperture is closed in response to increasing effective stress, regardless of whether the sample is single-fractured or double-fractured. The results indicate that the decrease in permeability is significant when the effective stress increases due to the increase of confining pressure. Furthermore, the increase in permeability is obvious when the effective stress decreases due to the increase of liquid pressure. The liquid pressure change has a greater effect on the permeability of fractured rock than confining pressure change.

3.3. PERMEABILITY TEST UNDER CYCLIC LOADING AND UNLOADING DEVIATORIC STRESS

A scheme of the permeability test for cyclic loading and unloading of deviatoric stress is shown in Figure 11. The confining pressure of 36 MPa and liquid pressure of 0.4 MPa were maintained constant throughout the cyclic tests. For S1, the permeability is decreased in the first two loading stages and then increased in the last two loading stages (Fig. 12). The permeability increases in the first two unloading stages and decreases in the last two unloading stages. The permeability of S2 decreases in the first three loading stage and then stabilises in the last loading stage. After the first deviatoric stress is loaded, a general compaction reduces the permeability rapidly because of the closure of the pre-existing fracture in

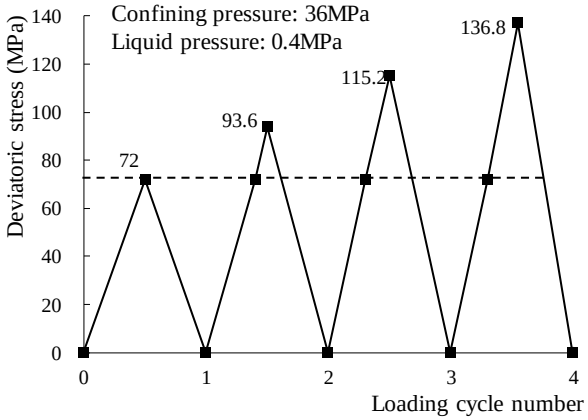

Fig. 11 Scheme of permeability test for cyclic loading and unloading of deviatoric stress.

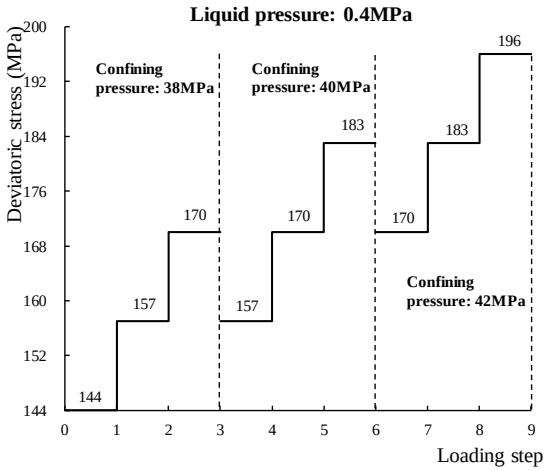

Fig. 13 Scheme of permeability test for increasing confining pressure and deviatoric stress.

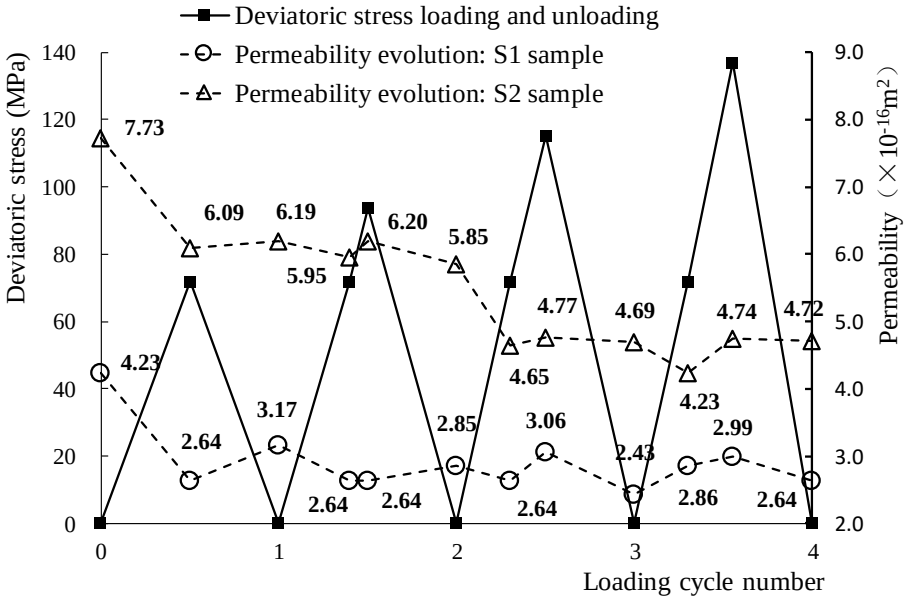

Fig. 12 Relationship between cyclic loading and unloading and permeability.

the samples. Partial fracture recovery results in increased permeability during the unloading process. In the following loading and unloading process, the fracture continues to compact under loading condition, enhancing the permeability reduction, and then partially recovers under unloading, causing a slow increase in permeability. However, the permeability is increased under high deviatoric stress loading because of fracture propagation and is decreased under unloading due to the fracture closure.

In general, the loading causes the change rate of permeability to decrease with the increase in the number of cycles. At the first loading stage, the aperture closure is significant and the change rate is large; as the number of cycles increases, the aperture continues to be compressed, and the change rate of permeability decreases and tends to stabilise. In addition, the increment is significantly smaller than the decrement during the cyclic tests, and the entire permeability evolution of the two samples is reduced. This result is due to the sample being strongly compacted in the initial loading phase and the closed crack unable to be reopened after unloading. The permeability has an evident loss, indicating that the cyclic loading and unloading causes irreversible compression of the sample.

3.4. PERMEABILITY TEST UNDER SYNCHRONOUSLY INCREASING CONFINING PRESSURE AND DEVIATORIC STRESS

A permeability test under synchronously increasing confining pressure and deviatoric stress was finally performed (Fig. 13). The confining pressure is increased from 38 MPa to 42 MPa, whereas the liquid pressure is kept constant at 0.4 MPa. Meanwhile, the deviatoric stress is increased from

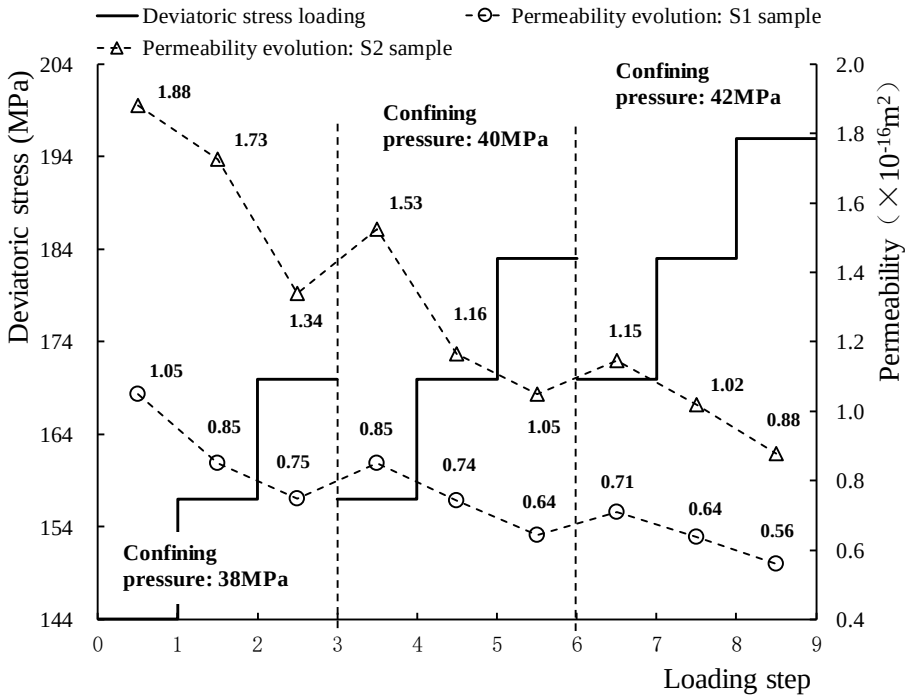

Fig. 14 Relationship between increasing confining pressure and deviatoric stress and permeability.

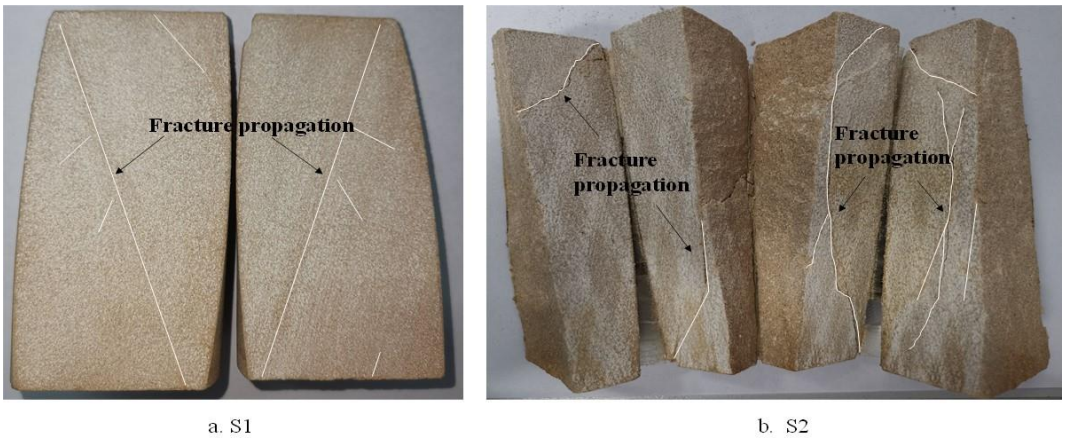

Fig. 15 Fracture propagation of the sample after permeability test.

144 MPa with an increment of 13 MPa until 196 MPa. Under different confining pressures, the permeability of the two samples is decreased with the increase of deviatoric stress (Fig. 14).

Given that the high deviatoric stress can reduce the fracture aperture width, the permeability decreases rapidly with the increase of deviatoric stress under low confining pressure. The permeability values decrease by 0.30×10^{-16} m^2 for S1 and 0.54×10^{-16} m^2 for S2 with the increase of the deviatoric stress under a confining pressure of 38 MPa. With the increase of confining pressure, the permeability of the two samples decreases slowly because of the continuous closure of the fracture and propagation of partial fracture. The permeability values decrease by 0.15×10^{-16} m^2 for S1 and 0.27×10^{-16} m^2 for S2 with the increase of the deviatoric stress under a confining pressure of 42 MPa. The permeability gap between S1 and S2 is decreasing. The result also indicates that the permeability change of the S2 sample is sensitive to the stress loading.

After the permeability test of different pressure conditions, the fracture propagations of S1 and S2 samples were obtained (Fig. 15). The shape of the fractures in S1 sample is relatively regular. The important shear crack and some branch cracks were observed, which appeared in parallel. The fracture propagation in S2 sample is more complex. The crack has obvious generation and propagation. A large number of tension and shear cracks were found under different pressure conditions. The dip angle of the shear fracture is about 45°, and the dip angle of the tension fracture ranges from 0° to 30°.

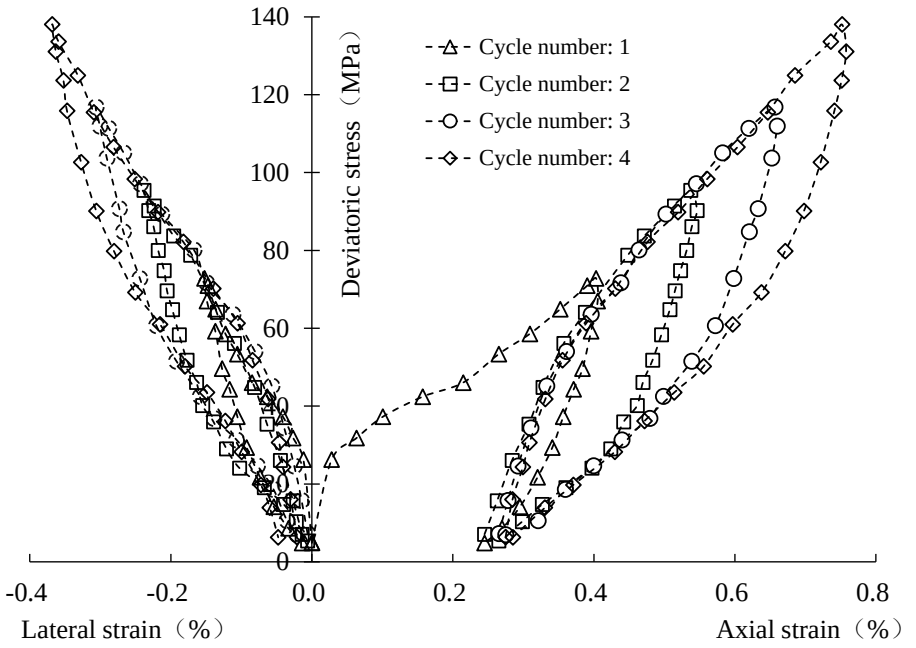

Fig. 16 Stress strain curve of S1 during cyclic loading and unloading deviatoric stress.

4. PERMEABILITY MODEL OF FRACTURED ROCK

4.1. MODEL OF SINGLE-FRACTURE PERMEABILITY

The permeability of fractured rock K consists of fracture permeability K_f and matrix permeability K_m expressed as follows:

$$K = K_f + K_m \tag{1}$$

Given that K_f is much larger than K_m. And the porosity of rock sample is 3.5 %, K_m can be considered constant during the test. The sample fracture deformation Δu_{fx} is the difference between the rock deformation Δu_x and matrix deformation Δu_{mx}.

$$\Delta u_{fx} = \Delta u_x - \Delta u_{mx} = L \cdot \Delta \varepsilon_x - (L-b) \cdot \Delta \varepsilon_{mx} \tag{2}$$

where L is the width of unit rock cell, b is the fracture width and $\Delta \varepsilon_x$ and $\Delta \varepsilon_{mx}$ are the rock strain and matrix strain in the horizontal direction. Therefore, the matrix deformation and fracture deformation can be obtained as follows:

$$\Delta u_{mx} = -\frac{L-b}{E_m}\left(\Delta \sigma_{ex} - \nu\left(\Delta \sigma_{ey} + \Delta \sigma_{ez}\right)\right) \tag{3}$$

$$\Delta u_{fx} = -\left(\frac{L}{E} - \frac{L-b}{E_m}\right)\left(\Delta \sigma_{ex} - \nu\left(\Delta \sigma_{ey} + \Delta \sigma_{ez}\right)\right) \tag{4}$$

where E and E_m are the elastic moduli of the rock and matrix, respectively. ν is Poisson's ratio; and $\Delta \sigma_{ex}$, $\Delta \sigma_{ey}$ and $\Delta \sigma_{ez}$ are the effective stresses in three directions.

The change of fracture deformation directly affects the permeability of the fracture. The single-fracture permeability can be obtained by relationship between fracture permeability and fracture width (Snow, 1965; Zimmerman and Bodvarsson, 1996).

$$dK_f = 2K_f\left(\frac{\Delta b}{b}\right) \tag{5}$$

where Δb is the fracture deformation, $\Delta b = \Delta u_{fx}$; and the fracture strain in the horizontal direction can be obtained as follows:

$$\frac{\Delta b}{b} = -\left[\frac{L}{b}\left(\frac{1}{E} - \frac{1}{E_m}\right) + \frac{1}{E_m}\right]\left[\Delta \sigma_{ex} - \nu\left(\Delta \sigma_{ey} + \Delta \sigma_{ez}\right)\right] \tag{6}$$

The permeability model of the single-fracture sample can be obtained as follows:

$$K_f = K_{f0} \cdot \exp\left\{-2\left[\frac{L}{b}\left(D - D_m\right) + D_m\right] \cdot \left[\sigma_{ex} - \nu\left(\sigma_{ey} + \sigma_{ez}\right)\right]\right\} \tag{7}$$

where K_{f0} is the permeability coefficient, and $D = 1/E$, $D_m = 1/E_m$, σ_{ex}, σ_{ey} and σ_{ez} are the external stresses in three directions, respectively.

During the stage of cyclic loading and unloading deviatoric stress, the stress-strain curves of S1 shows a significant volumetric dilatancy (Fig. 16). The volume change is mainly due to the expansion of the fracture and plastic behaviour under high deviatoric stress. Eq. (7) cannot effectively describe the

expansion deformation of fractures. Therefore, according to the Coulomb failure criterion, when the stress ratio γ of axial stress σ_{ey} to lateral stress σ_{ex} exceeds a critical value γ_c, the fracture starts to expand.

$$\gamma_c = \frac{1+\sin\theta}{1-\sin\theta} \tag{8}$$

where θ is the rock shear angle. The fracture expansion deformation Δd can be described by an exponential function and is mainly affected by the fracture width b and stress ratio γ (Min et al., 2004; Liu et al., 2016).

$$\Delta d = b \cdot \exp\left[\beta\left(\gamma-\gamma_c\right)\right] \qquad (\gamma > \gamma_c) \tag{9}$$

where β is the expansion coefficient. Therefore, the fracture strain in the horizontal direction can be rewritten as follows:

$$\frac{\Delta u_{fx}}{b} = -\left\{\left[\frac{L}{b}\left(\frac{1}{E}-\frac{1}{E_m}\right)+\frac{1}{E_m}\right]\left[\Delta\sigma_{ex}-\nu\left(\Delta\sigma_{ey}+\Delta\sigma_{ez}\right)\right]+\exp\left[\beta\left(\gamma-\gamma_c\right)\right]\right\} \tag{10}$$

Thus, the permeability model of the single-fracture sample is obtained when $\gamma > \gamma_c$.

$$K_f = K_{f0}\exp\left\{-2\left[\frac{L}{b}\left(D-D_m\right)+D_m\right]\left[\Delta\sigma_{ex}-\nu\left(\Delta\sigma_{ey}+\Delta\sigma_{ez}\right)\right]-\exp\left[\beta\left(\gamma-\gamma_c\right)\right]\right\} \tag{11}$$

4.2. MODEL OF MULTI-FRACTURE PERMEABILITY

The multi-fracture permeability K_f can be derived from dual-medium model (Harpalani and Chen, 1997).

$$dK_f = K_f\left(\frac{3\Delta b}{b}-\frac{\Delta\left(L-b\right)}{\left(L-b\right)}\right) \tag{12}$$

where Δb is the fracture deformation, Δb=Δu_{fx}; and $\Delta\left(L-b\right)$ is the matrix deformation, $\Delta\left(L-b\right)$=Δu_{mx}. Thus, the strain of fracture and matrix in the horizontal direction can be obtained as follows:

$$\frac{\Delta\left(L-b\right)}{L-b} = -\frac{1}{E_m}\left[\Delta\sigma_{ex}-\nu\left(\Delta\sigma_{ey}+\Delta\sigma_{ez}\right)\right] \tag{13}$$

$$\frac{\Delta b}{b} = -\frac{1}{b}\left(\frac{L}{E}-\frac{L-b}{E_m}\right)\left[\Delta\sigma_{ex}-\nu\left(\Delta\sigma_{ey}+\Delta\sigma_{ez}\right)\right] \tag{14}$$

The permeability model of the multi-fracture sample is obtained by integrating:

$$K_f = K_{f0}\cdot\exp\left\{-\left[\left(\frac{3\left(L-b\right)}{b}+1\right)\left(D-D_m\right)+2D\right]\left[\sigma_{ex}-\nu\left(\sigma_{ey}+\sigma_{ez}\right)\right]\right\} \tag{15}$$

where K_{f0} is the permeability coefficient, and $D=1/E$, $D_m=1/E_m$.

Similarly, given the expansion of the fracture, the stress strain curves of the S2 sample also show a significant volumetric dilatancy during cyclic loading and unloading deviatoric stress (Fig. 17). Therefore, the permeability model of the multi-fracture sample is obtained when $\gamma > \gamma_c$.

$$K_f = K_{f0}\exp\left\{-\left[\left(\frac{3(L-b)}{b}+1\right)\left(D-D_m\right)+2D\right]\left[\sigma_{ex}-\nu\left(\sigma_{ey}+\sigma_{ez}\right)\right]-3\exp\left[\beta\left(\gamma-\gamma_c\right)\right]\right\} \tag{16}$$

These models show an exponential relationship between permeability and changes in confining pressure, liquid pressure and deviatoric pressure, which are consistent with the experimental results obtained.

4.3. SIMULATION OF EXPERIMENTAL RESULTS

The model parameters mainly include two permeability parameters, K_{f0} and K_m; two elastic parameters, E and E_m; two fracture parameters, b and L, and one expansion parameter, β. In order to get a better

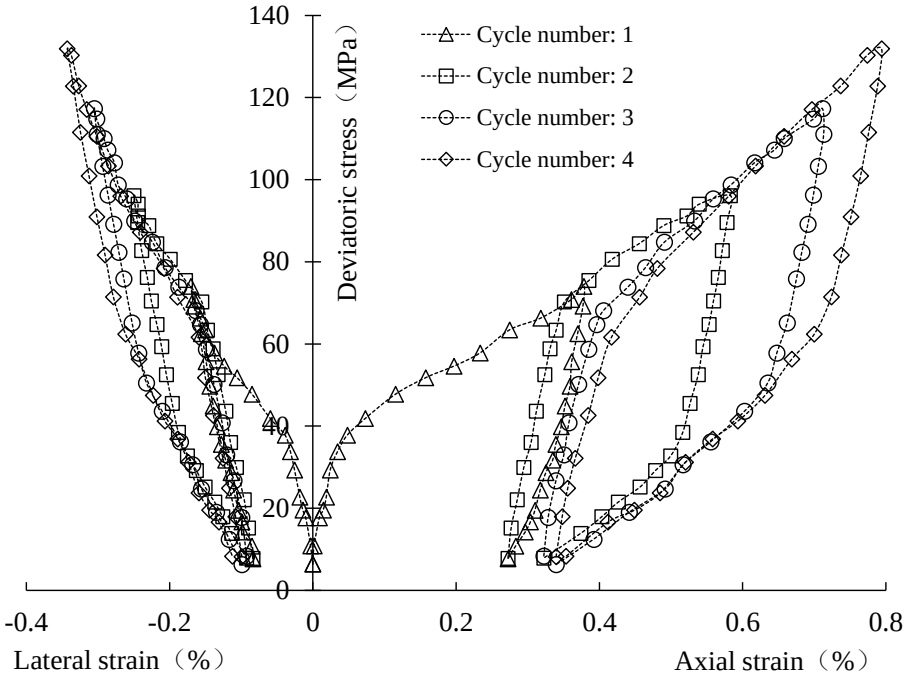

Fig. 17 Stress strain curve of S2 during cyclic loading and unloading deviatoric stress.

Table 1 Model parameters of permeability evolution model.

a. S1 sample

Stress path \ Model parameters		$\frac{L}{b}$	K_{f0} (m^2)	K_m (m^2)	D (MPa^{-1})	D_m (MPa^{-1})	β
Increasing confining pressure		1.03	6.89E-16	5.0E-17	0.02	0.21	
Increasing liquid pressure		0.29	2.19E-14		0.25	0.04	
Cyclic loading deviatoric stress	Second time loading	3.03	5.48E-16		0.55	0.83	3.52E-9
	Third time loading	1.98	6.55E-16		0.06	0.11	3.52E-9
	Fourth time loading	2.35	6.54E-16		0.21	0.37	3.54E-9
Increasing confining pressure and deviatoric stress	Confining pressure 38MPa	1.10	4.10E-16		0.01	0.99	3.17E-9
	Confining pressure 40MPa	6.93	3.42E-16		0.01	0.03	3.15E-9
	Confining pressure 42MPa	1.59	3.86E-16		0.20	0.72	3.62E-9

b. S2 sample

Stress path \ Model parameters		$\frac{L-b}{b}$	K_{f0} (m^2)	K_m (m^2)	D (MPa^{-1})	D_m (MPa^{-1})	β
Increasing confining pressure		0.43	1.56E-15	4.40E-17	0.03	0.04	
Increasing liquid pressure		0.09	8.47E-14		0.25	0.39	
Cyclic loading deviatoric stress	Second time loading	0.14	1.13E-14		0.11	0.27	3.47E-9
	Third time loading	0.46	8.42E-15		0.06	0.12	3.19E-9
	Fourth time loading	0.10	8.28E-15		0.16	0.40	3.10E-9
Increasing confining pressure and deviatoric stress	Confining pressure 38MPa	0.08	5.06E-15		0.10	0.33	3.36E-9
	Confining pressure 40MPa	0.63	5.52E-15		0.07	0.16	3.20E-9
	Confining pressure 42MPa	0.24	3.19E-15		0.22	0.52	3.25E-9

understanding on the performance of the model, the influence of model parameters on the permeability of fractured rock are studied. The influence of the permeability parameter K_{f0} and elastic parameter D are firstly studied (Figs. 18-19). The model results of single-fracture permeability and multi-fracture permeability show that fracture permeability K_f increase when K_{f0} and D increase. On the contrary, as the D_m, L/b and $(L-b)/b$ increase, the fracture permeability K_f decreases.

On the basis of the experimental results, the model parameters are calculated through global optimization algorithm. According to the nonlinear least squares method, the parameters obtained by iteration, and the permeability change of the two samples is simulated (Table 1). The simulations are

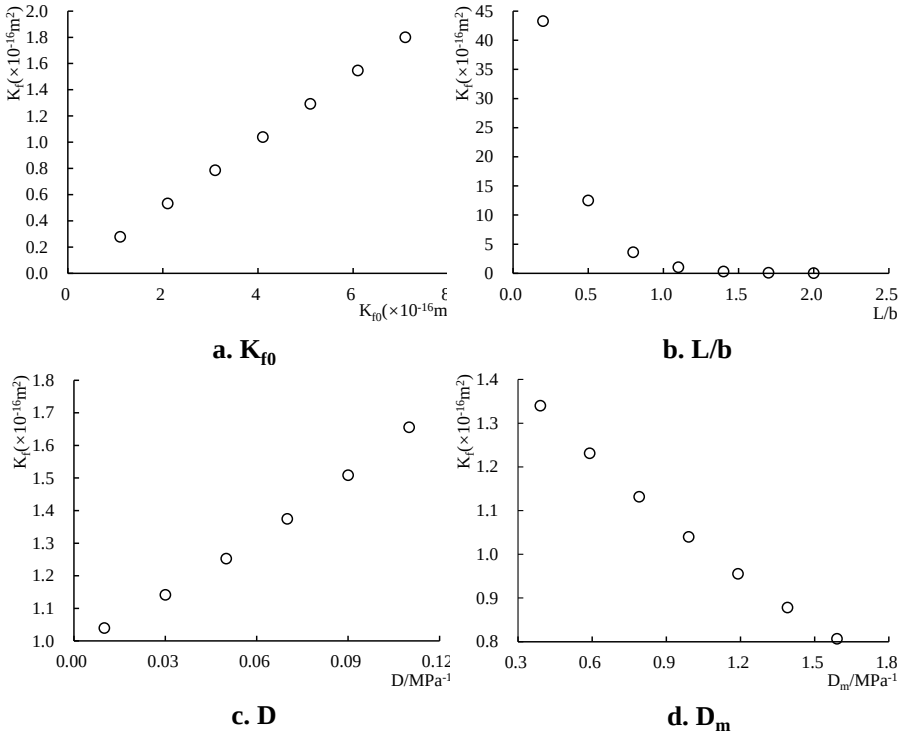

Fig. 18 Parameter sensitivity analysis of fracture permeability of S1.

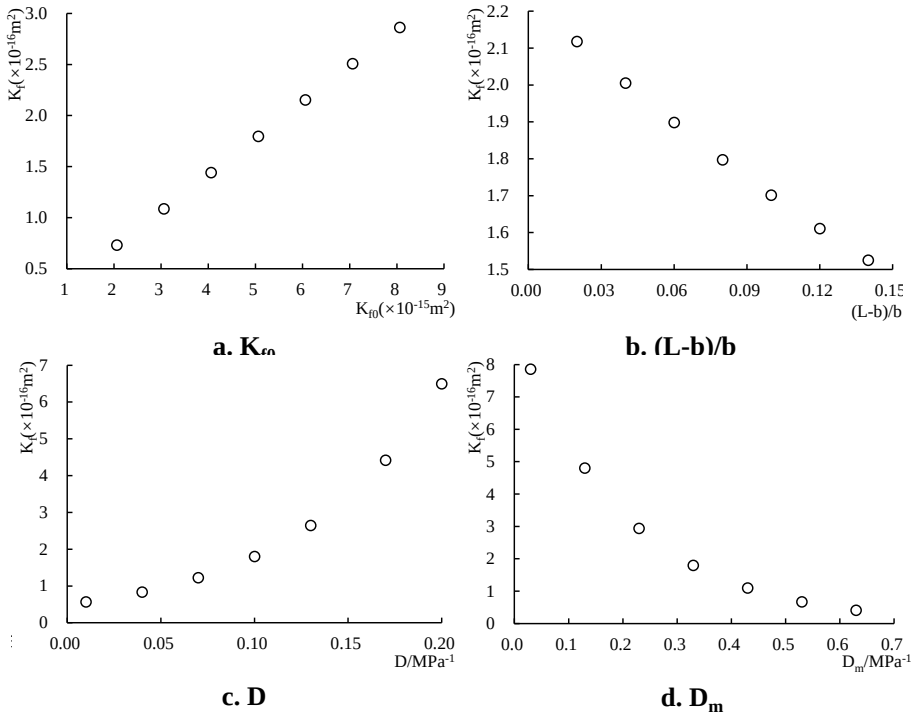

Fig. 19 Parameter sensitivity analysis of fracture permeability of S2.

performed on the permeability change during increasing confining pressure, increasing liquid pressure, cyclic loading deviatoric stress and synchronously increasing confining pressure and deviatoric stress. The stage of cyclic unloading deviatoric stress was not simulated because only a few measurement points are available. The simulation results are in good agreement with the experimental results (Figs. 20-21). The permeability model can describe the permeability evolution of fractured rock in different pressure conditions.

5. CONCLUSIONS

Based on the test results, the permeability of fractured rock samples in different pressure conditions was analysed in detail. The main conclusions are as follows:

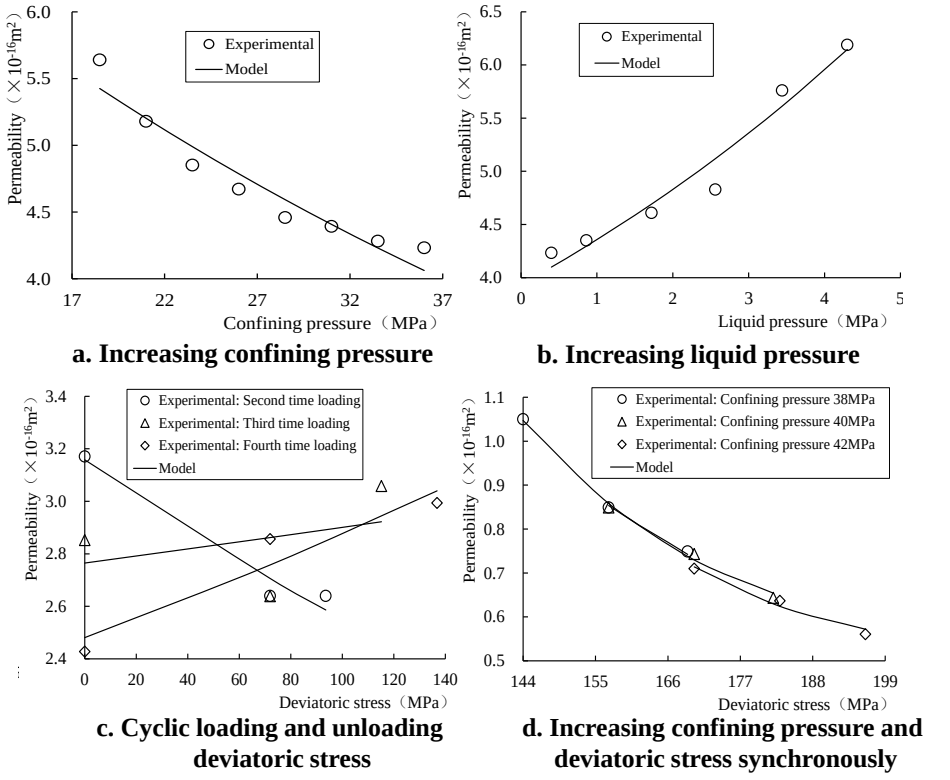

a. Increasing confining pressure **b. Increasing liquid pressure**

c. Cyclic loading and unloading deviatoric stress **d. Increasing confining pressure and deviatoric stress synchronously**

Fig. 20 Simulation results of permeability evolution of S1.

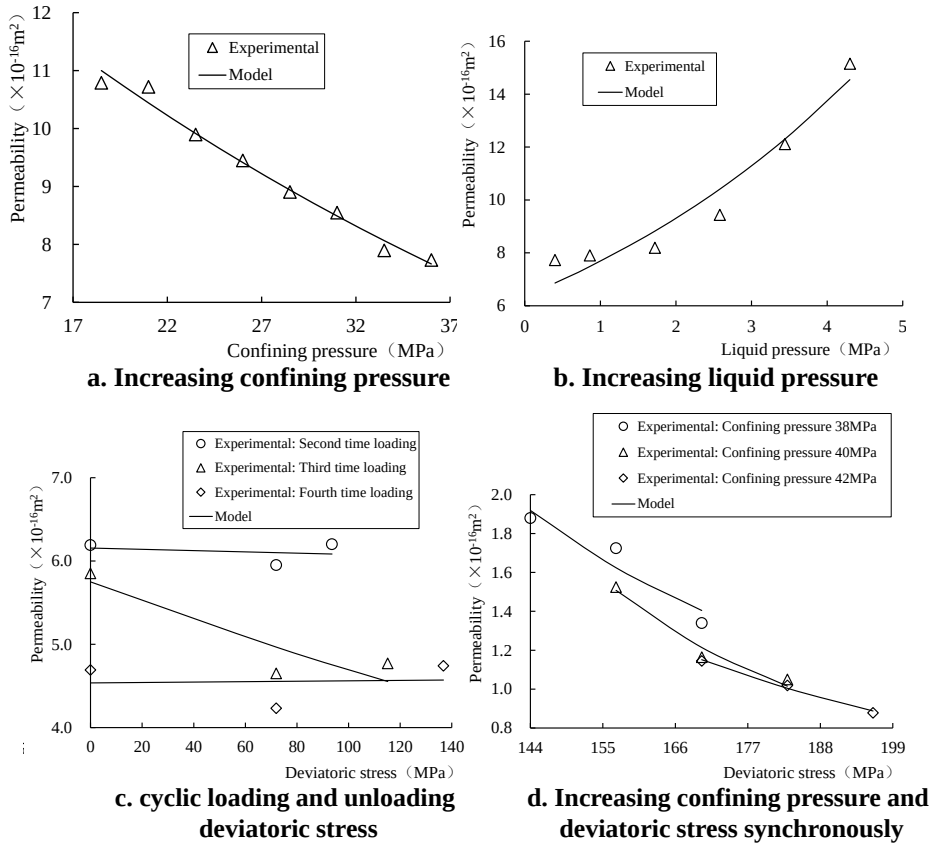

a. Increasing confining pressure **b. Increasing liquid pressure**

c. cyclic loading and unloading deviatoric stress **d. Increasing confining pressure and deviatoric stress synchronously**

Fig. 21 Simulation results of permeability evolution of S2.

- The permeability of fractured rock is strongly dependent on the change of pressure. The permeability decreases exponentially with the increase of confining pressure but increases exponentially with the increase of liquid pressure. Moreover, the permeability change under increasing liquid pressure is significantly higher than that under increasing confining pressure.
- Under low deviatoric stress, the loading and unloading causes a decrease and increase in the permeability. However, under high deviatoric stress, the permeability increases under loading and decreases under unloading. The cyclic loading and unloading irreversibly compress the sample. Furthermore, the permeability decreases with the synchronous increase of confining pressure and deviatoric stress.
- The permeability model of single fracture and multi-fracture are proposed considering the interaction among fracture system, matrix system and expansion deformation of fracture under external stress. The models can effectively describe the permeability change of fractured rock in different pressure conditions.

ACKNOWLEDGEMENTS

The financial support provided by China Natural Science Foundation (No. 51890914), Natural Science Foundation of Shandong Province (No. ZR2019MEE001) and Opening Foundation of Shandong Key Laboratory of Civil Engineering Disaster Prevention and Mitigation (CDPM2019KF01) is gratefully acknowledged. The authors wish to thank the two reviewers and the editor for their kind advice, which has significantly enhanced the soundness of this paper.

REFERENCES

Abass, H.H., Khan, M.R. and Sierra, L.: 2009, Understanding stress sensitive tight gas reservoirs. Saudi Aramco J. Technol. Summer edition, 11–21.

Alexandra, R.L.K., Michael, J.H. and Patrick, B.: 2018, Assessing the role of fractures on the permeability of the Permo-Triassic sandstones at the Soultz-sous-Forêts (France) geothermal site. Geothermics, 74, 181–189. DOI: 10.1016/j.geothermics.2018.03.009.

Brace W.F.: 1978, A note on permeability changes in geologic material due to stress. Pure and Applied Geophysics, 116, (4-5), 627–633. DOI: 10.1007/BF00876529

David, C., Menendez, B., Zhu, W. and Wong, T.F.: 2001, Mechanical compaction, microstructures and permeability evolution in sandstones. Phys. Chem. Earth, (A), 26, 1-2, 45–51. DOI: 10.1016/S1464-1895(01)00021-7

Durant, B., Abualfaraj, N., Olson, M.S. and Gurian, P.L.: 2016, Assessing dermal exposure risk to workers from flowback water during shale gas hydraulic fracturing activity. J. Nat. Gas Sci. Eng., 34, 969–978. DOI: 10.1016/j.jngse.2016.07.051

Estrada, J.M. and Bhamidimarri, R.: 2016, A review of the issues and treatment options for wastewater from shale gas extraction by hydraulic fracturing. Fuel, 182, 292–303. DOI: 10.1016/j.fuel.2016.05.051

Farquharson, J.I., Heap, M.J. and Baud, P.: 2016, Strain-induced permeability increase in volcanic rock. Geophys. Res. Lett., 43, 22, 11603–11610. DOI: 10.1002/2016GL071540

Gutierrez, M. and Lewis, R.: 2002, Coupling of fluid flow and deformation in underground formations. J. Eng. Mech., 128, 7, 779–787. DOI: 10.1061/(ASCE)0733-9399(2002)128:7(779)

Harpalani, S. and Chen, G.L.: 1997, Influence of gas production induced volumetric strain on permeability of coal. Geotech. Geol. Eng., 15, 4, 303–325. DOI: 10.1007/BF00880711

Heap, M., Reuschlé, T., Baud, P., Renard, F. and Iezzi, G.: 2018, The permeability of stylolite-bearing limestone. J. Struct. Geol., 116, 81–93. DOI: 10.1016/j.jsg.2018.08.007

Heiland, J. and Raab, S.: 2001, Experimental investigation of the influence of differential stress on permeability of a Lower Per mian (Rotliegend) sandstone deformed in the brittle deformation field. Phys. Chem. Earth, (A), 26, 1-2, 33–38. DOI: 10.1016/S1464-1895(01)00019-9

Heiland, J.: 2003, Laboratory testing of coupled hydro-mechanical processes during rock deformation. Hydrogeol. J., 11, 1, 122–141. DOI: 10.1007/s10040-002-0236-2

Huo, D. and Benson, S.M.: 2016, Experimental investigation of stress-dependency of relative permeability in rock fractures. Transp. Porous Media, 113, 567–590. DOI: 10.1007/s11242-016-0713-z

Katsuki, D., Gutierrez, M. and Almrabat, A.: 2019, Stress-dependent shear wave splitting and permeability in fractured porous rock. J. Rock Mech. Geotech. Eng., 11, 1–11. DOI: 10.1016/j.jrmge.2018.08.004

Liang, M.L., Wang, Z.X., Zhang, Y., Greenwell, C.H., Li, H.J., Yu, Y.X. and Liu, S.X.: 2021, Experimental investigation on gas permeability in bedding shale with brittle and semi-brittle deformations under triaxial compression. J. Pet. Sci. Eng., 196, 108049. DOI: 10.1016/j.petrol.2020.108049

Liu, W., Li, Y. and Wang, B.: 2010, Gas permeability of fractured sandstone/coal samples under variable confining pressure. Transp. Porous Media, 83, 2, 333–347. DOI: 10.1007/s11242-009-9444-8

Liu, R.C., Li, B. and Jiang, Y.J.: 2016, A fractal model based on a new governing equation of fluid flow in fractures for characterizing hydraulic properties of rock fracture networks. Comput. Geotech., 75, 57–68. DOI: 10.1016/j.compgeo.2016.01.025

Liu, Z.B., Shao, J.F., Xie, S.Y. and Secq, J.: 2015, Gas permeability evolution of clayey rocks in process of compressive creep test. Mater. Lett., 139, 1, 422–425. DOI: 10.1016/j.matlet.2014.10.139

Ma, Y.Q., Zhang, Y.J., Huang, Y.B., Zhang, Y. and Huang, Z.J.: 2019, Experimental study on flow and heat transfer characteristics of water flowing through a rock fracture induced by hydraulic fracturing for an

enhanced geothermal system. Appl. Therm. Eng., 154, 433–441.
DOI: 10.1016/j.applthermaleng.2019.03.114

Min, K.B., Rutqvist, J.,Tsang, C. F., et al.: 2004, Stress-dependent permeability of fractured rock masses: a numerical study. Int. J. Rock Mech. Min. Sci., 41, 7, 1191–1210. DOI: 10.1016/j.ijrmms.2004.05.005

Mitchell, T.M. and Faulkner, D.R.: 2008, Experimental measurements of permeability evolution during triaxial compression of initially intact crystalline rocks and implications for fluid flow in fault zones. J. Geophys. Res., 113, B11412.
DOI: 10.1029/2008JB005588

Snow, D.T.: 1965, A parallel plate model of fractured permeable media. Ph.D. Dissertation, University of California.

Sheng, J., Soliman, M. and Wan, T.: 2013, Study evaluates EOR potential in naturally fractured shale reservoirs. December 2013 Exclusive Story, the American Oil and Gas Reporter.

Shu, B., Zhu, R.J., Elsworth, D., Dick, J., Liu, S., Tan, J.Q. and Zhang, S.H.: 2020, Effect of temperature and confining pressure on the evolution of hydraulic and heat transfer properties of geothermal fracture in granite. Appl. Energy, 272, 115290.
DOI: 10.1016/j.apenergy.2020.115290

Souley, M., Homand, F., Pepa, S. and Hoxha, D.: 2001, Damage-induced permeability changes in granite: a case example at the URL in Canada. Int. J. Rock Mech. Min. Sci., 38, 2, 297–310.
DOI: 10.1016/S1365-1609(01)00002-8

Wanniarachchi, W.A.M., Ranjith, P.G., Perera, M.S.A., Rathnaweera, T.D., Zhang, D.C. and Zhang, C.: 2018, Investigation of effects of fracturing fluid on hydraulic fracturing and fracture permeability of reservoir rocks: An experimental study using water and foam fracturing. Eng. Fract. Mech., 194, 117–135.
DOI: 10.1016/j.engfracmech.2018.03.009

Wang, H.L., Xu, W.Y., Shao, J.F. and Skoczylas, F.: 2014, The gas permeability properties of low-permeability rock in the process of triaxial compression test. Mater. Lett., 116, 2, 386–388. DOI: 10.1016/j.matlet.2013.11.061

Wang, G., Wang, K., Wang, S.G., Elsworth, D. and Jiang, Y.J.: 2018, An improved permeability evolution model and its application in fractured sorbing media. J. Nat. Gas Sci. Eng., 56, 222–232.
DOI: 10.1016/j.jngse.2018.05.038

Yang, D.S., Billiotte, J. and Su, K.: 2010, Characterization of the hydromechanical behavior of argillaceous rocks with effective gas permeability under deviatoric stress. Eng. Geol., 114, 116–122.
DOI: 10.1016/j.enggeo.2010.04.002

Yang, R., Ma, T.R., Liu, W.Q., Fang, Y.J. and Xing, L.Y.: 2019 Coupled hydro-mechanical analysis of gas production in fractured shale reservoir by random fracture network modeling. Int. J. Appl. Mech., 11, 03, 1950031. DOI: 10.1142/S1758825119500315

Zhang, J., Standifird, W.B., Roegiers, J.C. and Zhang, Y.: 2007, Stress dependent fluid flow and permeability in fractured media: from lab experiments to engineering applications. Rock Mech. Rock Eng., 40, 1, 3–21. DOI: 10.1007/s00603-006-0103-x

Zhang, Y.J., Ma, Y.Q., Hu, Z.J., Lei, H.L., Bai, L., Lei, Z.H. and Zhang, Q.: 2019, An experimental investigation into the characteristics of hydraulic fracturing and fracture permeability after hydraulic fracturing in granite. Renew. Energy, 140, 615–624.
DOI: 10.1016/j.renene.2019.03.096

Zhao, Y., Wang, C.L., Zhao, Y.L., He, L., Wan, W. and Zhang, Y.F.: 2019, Experimental characterization and dependence of rock fracture permeability on 3D stresses. Arab. J. Geosci., 12, 41, 1–9.
DOI: 10.1007/s12517-018-4200-4

Zhu, W. and Wong, T.: 1997, The transition from brittle faulting to cataclastic flow: permeability evolution. J. Geophys. Res., 102, 3027–3041.
DOI: 10.1029/96JB03282

Zhang, Y., Liu, Z.B., Xu, W.Y. and Shao, J.F.: 2015, Change in the permeability of clastic rock during multi-loading triaxial compressive creep tests. Geotech. Lett., 5, 7-9, 167–172. DOI: 10.1680/jgele.15.00029

Zhang, Y., Shao, J.F., Xu, W.Y. and Jia, Y.: 2016, Time-dependent behavior of cataclastic rocks in a multi-loading triaxial creep test. Rock Mech. Rock Eng., 49, 9, 3793–3803. DOI: 10.1007/s00603-016-0948-6

Zimmerman, R.W. and Bodvarsson, G.S.: 1996, Hydraulic conductivity of rock fractures. Transp. Porous Media, 23, 1, 1–30. DOI: 10.1007/BF00145263